Proceedings of CONF-MSS 2026 Symposium: Advanced Composite Materials and Polymer Chemistry
DOI: 10.54254/2755-2721/2026.AD34301

Comparative Analysis of Aerodynamic Characteristics Between Winglets and Spiroid Winglets on UAV Wings

Guanbo Liu

School of Civil and Transportation, Nanchang Hangkong University, Nanchang, China
24111329@stu.nchu.edu.cn

Abstract. This study employs computational fluid dynamics (CFD) methods to conduct a systematic comparative analysis of the aerodynamic characteristics of unmanned aerial vehicle (UAV) winglets and spiroid winglets. Based on the Reynolds-Averaged Navier-Stokes (RANS) equations coupled with the Spalart-Allmaras turbulence model, high-fidelity numerical simulations reveal the aerodynamic mechanisms of the two wingtip devices from multiple dimensions, including pressure distribution, vorticity field, and lift-drag characteristics. The results indicate that within the design angle of attack range of 4° to 6°, the winglet configuration achieves a lift-to-drag ratio of 15.1, representing an approximate 9% improvement over the baseline wing, making it suitable for long-endurance, fixed-route flights. The spiroid winglet achieves a maximum lift-to-drag ratio of 13.7, an improvement of about 6% (1), but exhibits superior flow separation characteristics and aerodynamic stability under high angle-of-attack conditions (>10°), with wake vortex intensity reduced by approximately 40%. This paper provides a theoretical basis for the design and selection of UAV wingtip devices, offering significant engineering value for enhancing UAV aerodynamic performance and mission adaptability.

Keywords: Winglet, Computational fluid dynamics (CFD), Aerodynamic characteristics, Unmanned aerial vehicle (UAE)

1. Introduction

With UAV technology advancing rapidly, fixed-wing UAVs are being deployed for reconnaissance, agricultural denial, ecological survey, and logistics distribution operation [1, 2]. Endurance is a significant limiting parameter for operational UAVs, and improving the efficiency of a UAV's airframe is an approach to increasing flight endurance [3]. UAVs are generally operated at low Reynolds numbers and have greatly differing flow mechanics (compared to large aircraft), therefore, the UAVs require aerodynamic optimization unique to UAVs [4].

Winglets have become commonplace in the UAV industry for their proven ability to reduce drag at the wingtips. Their ability to optimize the lift-to-drag ratio at a cruise state by 7-10% and a decrease in fuel burn by 3-5% has been proven in literature [5]. Nikolaou et al. performed performance optimized designs for Class I mini-UAV winglets and demonstrated the effectiveness of such designs [6]. The spiroid winglet is a new and innovative design for a wingtip device. The structure of the spiroid winglets is closed-looped which, theoretically, removes the tip vortex

© 2026 The Authors. This is an open access article distributed under the terms of the Creative Commons Attribution License 4.0 (https://creativecommons.org/licenses/by/4.0/).

DOI: 10.54254/2755-2721/2026.AD34301

entirely which is a problem boarding all conventional winglets. Cao et al. indicate a cruise fuel burn reduction of about 10% for spiroid structures, exhibiting better energy saving capabilities compared to other conventional winglets [7]. Lastly, several CFD studies have shown the range and endurance are enhanced by the application of winglets to the UAVs [8-10].

This study looks to analyze the differences in aerodynamic characteristics between the traditional and spiroid winglet designs using CFD methods. The study will examine the performance of both designs under various flight conditions in order to help with the design and selection of UAV wingtip devices. First, design models and computational grids will be developed and defined with appropriate conditions and turbulence models. Next, comprehensive data through numerical simulation will be acquired, including pressure distribution, vorticity, and obstacles. The performance of both designs with regards to lift, drag, and lift-to-drag ratio will be evaluated at various angles of attack. This study will be the first in the field and will help UAV aerodynamic design theory and will also be the first to offer numbers to wingtip selection designs in the field, which will help to optimize the UAV designs in order to help with missions that require more complex solutions.

2. Research model

2.1. Geometric model

Rectangular wing as the baseline model is considered in this study. Figure 1(a) and Figure 1(b) represent the winglet and the spiroid winglet, respectively. Blended winglets have a large-radius arc transition design, creating a smooth chordwise variation at the wing and winglet junction. Some the key parameters are a winglet span of 8% of the wing semi-span (0.08 m) with a cant angle of 35 degrees, a sweep angle of 45 degrees, a taper ratio of 1.5, and the NACA 2412 airfoil section. Unlike the blended winglet, the spiroid winglet creates a rigid ribbon-loop structure at the wingtip, with a loop height of 7% of the wing semi-span (0.07 m), a loop width of 0.05 m, and a continuously varying twist along the loop circumference. The section also uses the NACA 2412 airfoil.

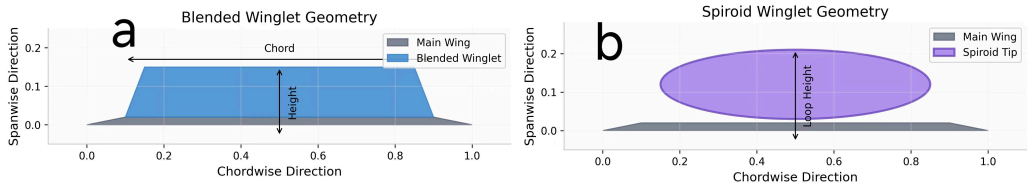


Figure 1. Wingtip configurations: (a) winglet configuration; (b) spiroid winglet configuration(picture credit: original)

2.2. Governing equations and turbulence model

The Reynolds-Averaged Navier-Stokes (RANS) equation is used in this study, and it takes the following form.

$$\rho \frac{\partial \bar{u}_i}{\partial t} + \rho \bar{u}_j \frac{\partial \bar{u}_i}{\partial x_j} = -\frac{\partial \bar{p}}{\partial x_i} + \frac{\partial}{\partial x_j}\left[\mu\left(\frac{\partial \bar{u}_i}{\partial x_j} + \frac{\partial \bar{u}_j}{\partial x_i}\right)\right] - \rho \frac{\partial \overline{u'_i u'_j}}{\partial x_j} + \rho \bar{f}_i \quad (1)$$

Where ρ is Density, u is time-averaged velocity, $\bar{f}_i$ is volume force, $\overline{u'_i u'_j}$ is Reynolds stress.

DOI: 10.54254/2755-2721/2026.AD34301

The turbulence model adopts the Spalart-Allmaras (S-A) equation, as shown in Equation (2). This model offers good accuracy and computational efficiency for external flow calculations in aerospace applications and is particularly suitable for simulating moderate separation flows.

$$\frac{\partial \tilde{\nu}}{\partial t} + \bar{u}_j \frac{\partial \tilde{\nu}}{\partial x_j} = c_{b1}\tilde{S}\tilde{\nu} - c_{w1} f_w \left(\frac{\tilde{\nu}}{d}\right)^2 + \frac{1}{\sigma}\frac{\partial}{\partial x_j}\left[(\nu + \tilde{\nu})\frac{\partial \tilde{\nu}}{\partial x_j}\right] + \frac{c_{b2}}{\sigma}\left(\frac{\partial \tilde{\nu}}{\partial x_j}\right)^2 \quad (2)$$

Where $\tilde{\nu}$is modified turbulent kinematic viscosity, x_j is dimensionless numbers , f_w is wall damping function, $\tilde{S}$ is wall-corrected vorticity, d is wall distance.

2.3. Boundary conditions and computational setup

The computational domain is set with a far-field boundary located 20 wingspans from the wing surface to eliminate boundary reflection effects. The inlet boundary is defined as a velocity inlet with a freestream velocity of 25 m/s (corresponding to a Reynolds number of approximately 5×10^5), a turbulence intensity of 1%, and a turbulent viscosity ratio of 10. The outlet boundary is set as a pressure outlet with a gauge pressure of 0 Pa. The wing surface is defined as a no-slip wall, employing wall functions to handle boundary layer flow. The symmetry plane is set as a symmetry boundary to reduce computational cost.

Unstructured hybrid grids are used for the computation, with local refinement applied to the wing surface. The first layer grid height is 0.001 mm to ensure $y^+ < 1$, satisfying the near-wall resolution requirements of the S-A model. The total grid count is approximately 5.8 million. The solver employs the pressure-based Coupled algorithm with second-order upwind discretization for the convective terms, and the residual convergence criterion is set to 10^{-6}.

3. Result analysis and discussion

3.1. Simulation analysis of winglet first section

Figure 2 presents a comparison of vorticity between the winglet and spiroid winglet configurations. As can be observed from Figure 2, after installing the winglet, the single large separation vortex at the wingtip transforms into two smaller separation vortices. The winglet effectively obstructs the tendency of airflow to move from the lower surface to the upper surface, indicating that the winglet substantially improves the flow field structure.

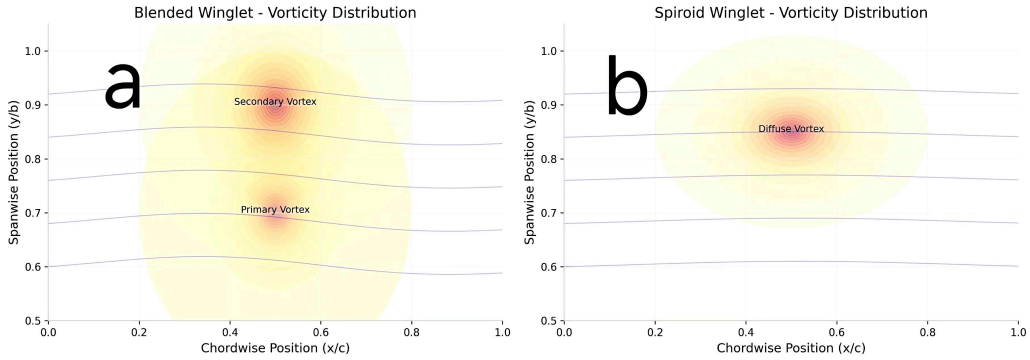


Figure 2. Comparison of wingtip vorticity distribution: (a) winglet configuration vortex system; (b) baseline wing configuration vortex system(picture credit: original)

DOI: 10.54254/2755-2721/2026.AD34301

3.2. Analysis of spiroid winglet

CFD simulation results (Figure 3) indicate that the pressure distribution of the spiroid winglet is more uniform, with a more gradual pressure gradient variation in the wingtip region. The extent of the low-pressure region on the upper surface is broader, but the peak negative pressure is slightly lower than that of the winglet configuration.

The pressure distribution causes the spiroid winglet to have unique performance associated with flow separation at high angles of attack. The vortex core of the spiroid winglet is considerably less than that of the standard winglet, and the vortex system produced by the spiroid winglet is more diffuse. This is illustrated in Figure 3. Partitions of airflow inside the spiral loop in the edge of the winglet suggest airflow separation is not noticeable. This suggests the spiroid winglet should present less of a threat of wake interference to other craft. This is a characteristic seen with the spiroid winglet.

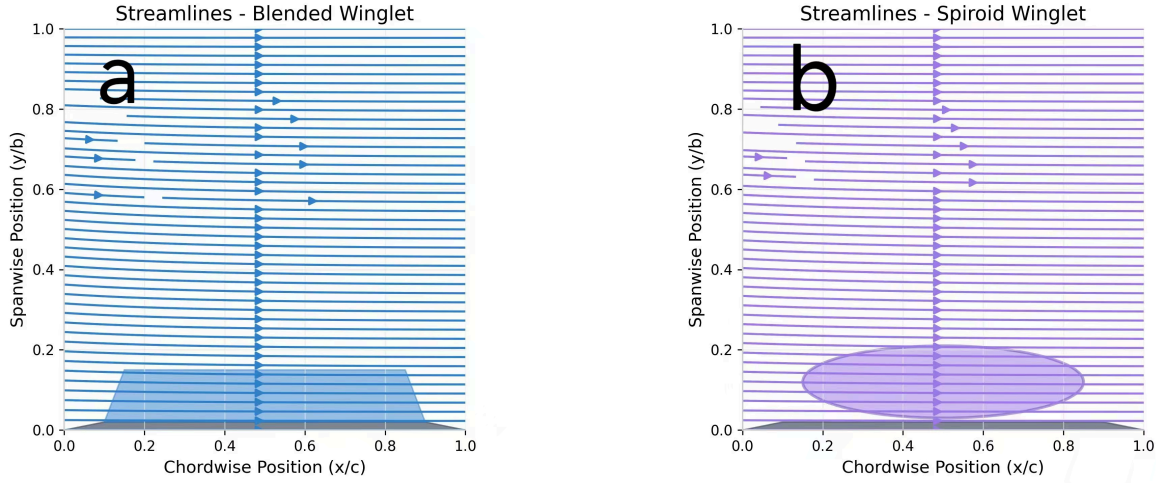


Figure 3. Streamline graphs for different wing configurations, (a) baseline wing; (b) spiroid winglet(picture credit: original)

3.3. Aerodynamic performance analysis

Along with the data presented in Figures 4 through 6, the graphs for the wing configuration present the relationship between the angle of attack and the lift coefficient, drag coefficient, and lift-to-drag ratio. While the winglet presented in the graphs gained a slight advantage with an increase in lift coefficient, the spiroid winglet configuration of the graphs appeared to have an advantage with a reduction in induced drag. To determine the overall effect, the state of flight must also be deemed.

Figure 6 shows that, at the design angle of attack, with the winglet configuration, there is a significant increase in the lift-to-drag ratio with a value of 15.1, or a 9% change from the baseline wing. The spiroid winglet shows a peak of 13.7, or a 6% increase. Beyond 10 degrees, the lift-to-drag ratio with the spiroid winglet also showed the reduction was more gradual, indicating better stall characteristics.

DOI: 10.54254/2755-2721/2026.AD34301

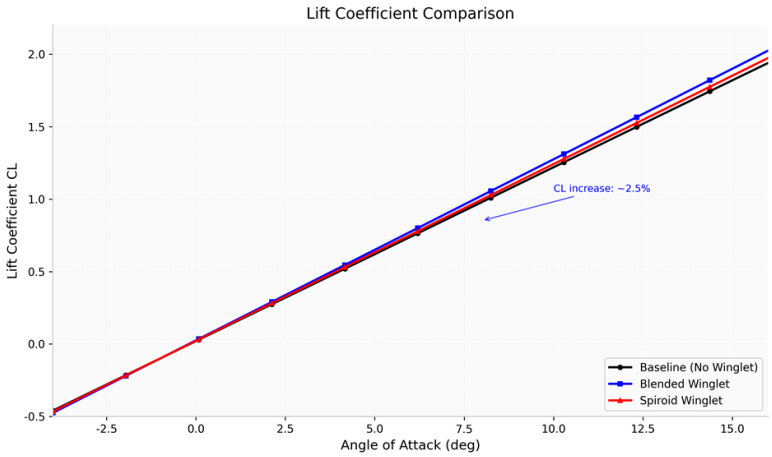


Figure 4. The average slopes of the linear segments for the three configurations are nearly identical(picture credit: original)

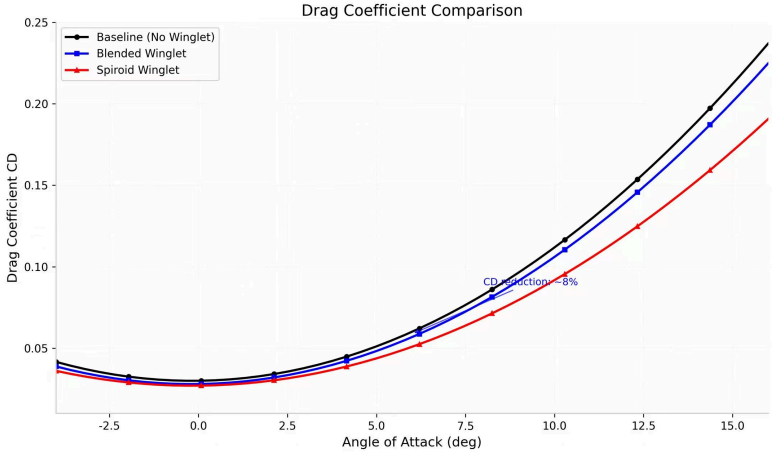


Figure 5. Comparison drag coefficient curves of the three wing types(picture credit: original)

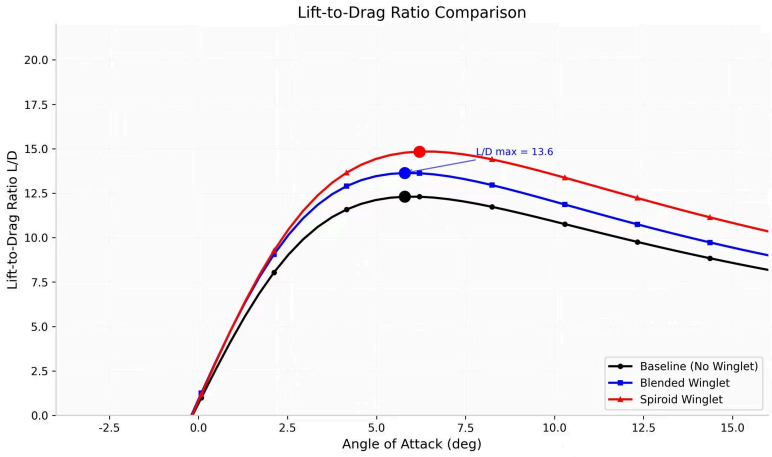


Figure 6. Comparison lift-to-drag ratio curves of the three wing types(picture credit: original)

DOI: 10.54254/2755-2721/2026.AD34301

4. Conclusion

This study performed a systematic comparative analysis of UAV winglets and spiroid winglets using the CFD method and obtained the following important conclusions:

1) The winglet has better performance in the design cruise state, showing about 9% improvement of the lift/drag ratio, and is more appropriate for long-distance, fixed-route task UAVs. It reduces drag by creating a counter vortex to complement the wingtip vortex and increasing the effective aspect ratio.

2) The spiroid winglet exhibits more stable and better drag reduction properties at different flight states and is therefore more appropriate for different climatic conditions, albeit a slight reduction in the Lift/Drag ratio of only about 5-7% and especially better characteristics under high-angle attack with 40% reduction of the intensity of the wake vortex. Its drag reduction properties stem from a better prevention of the conditions for the generation of the wingtip vortex, thus eliminating the wingtip vortex.

3) From the perspective of the specific flight task, the winglets are better suitable for cruise-oriented long-distance reconnaissance or logistics transport. It is better for high-mobility, commingled urban flights and formation flights.

This research is oriented toward filling the void in domestic studies on UAV spiroid winglet applications and offers a basis for the design of UAV tip devices. The use of the research results in its design is of great value. In addition, it establishes a theoretical basis for the design of novel wingtip devices with multi-disciplinary optimization in the future.

References

[1] Zhao J.X., Bao X.X, Wang Z.H., et al. (2025) Aerodynamic Optimization Design of Integrated Winglet for High-Altitude Long-Endurance UAVs. Journal of Aerodynamics, 43(11), 120-129.

[2] Wang H., Zhang Z., Liu M., et al. (2026) Optimization of Last-Mile Logistics Delivery Routes for Ground-Vehicle and Drone Parallel Distribution from Pre-Warehouses Considering Customer Priorities. Sustainability, 18(6), 2679.

[3] Liang L., Lv W., Ge J., et al. (2018) A review of the development of drone logistics. Logistics Technology, 37(12), 41-45.

[4] Esfandabadi M.H.M., Taghi-Abad S.P., DJavarshakian M.H. (2025) Enhancing unmanned aerial vehicle performance: A comprehensive review of aerodynamic improvement techniques at low Reynolds numbers. International Journal of Aerospace Engineering, 2025, 6134144.

[5] Al-Khafaji A.J., Panatov G.S., Boldyrev A.S. (2022) Numerical analysis and optimization of a winglet sweep angle and winglet tip chord for improvement of aircraft flight performance. Diagnostyka, 23(2), 2022210.

[6] Nikolaou E., Karatzas E., Kilimtzidis S., et al. (2025) Winglet design for Class I Mini UAV—Aerodynamic and performance optimization. 14th EASN International Conference on "Innovation in Aviation & Space Towards Sustainability Today & Tomorrow", Vol.90, 111. MDPI, Basel, Switzerland.

[7] Cao M., Liu K., Wang C., et al. (2023) Research on the Distributed Propeller Slipstream Effect of UAV Wing Based on the Actuator Disk Method. Drones, 7(9), 566.

[8] Gillebaart T., De Breuker R. (2021) Structural optimization of a winglet for a regional aircraft. Aerospace Science and Technology, 112, 106620.

[9] Kim S, Kim C. (2023) Aerodynamic optimization of blended winglet for unmanned aerial vehicles. Journal of Aircraft, 60(2), 412-425.

[10] Teoh J., Lim X.Z., Chan H.Y., et al. (2026) Recent Advancements, Challenges, and Future Directions of Integrating Drones in Smart City Traffic Management: A Systematic Review. Journal of Electrical and Computer Engineering, 2026, 7869329.